One Ring to Bind Them All: Shape-Selective Complexation of Phenylenediamine Isomers with Cucurbit[6]uril in the Gas Phase

David V. Dearden,*,† Tyler A. Ferrell,† Matthew C. Asplund,† Lloyd W. Zilch,‡ Ryan R. Julian,§ and Martin F. Jarrold‡

Department of Chemistry and Biochemistry, C100 Benson Science Building, Brigham Young University, Provo, Utah 84602-5700, Department of Chemistry and Biochemistry, University of Indiana, and University of California, Riverside

Received: October 3, 2008; Revised Manuscript Received: December 2, 2008

We examined complexes between cucurbit[6]uril and each of *ortho*-, *meta*-, and *para*-phenylenediamine using computational methods, Fourier transform ion cyclotron resonance mass spectrometry, and ion mobility spectrometry. These fundamental gas phase studies show that the lowest energy binding sites for *ortho*- and *meta*-phenylenediamine are on the exterior of cucurbit[6]uril, whereas *para*-phenylenediamine preferentially binds in the interior, in a pseudorotaxane fashion. This conclusion is based on reactivity of each of the complexes with *tert*-butylamine, where the *ortho*- and *meta*-phenylenediamine complexes exchange with *tert*-butylamine, whereas the *para*-phenylenediamine complex undergoes two slow additions without displacement. Further, under sustained off-resonance irradiation conditions, the *ortho*- and *meta*-phenylenediamine complexes fragment easily via losses of neutral phenylenediamine, whereas the *para*-phenylenediamine complex fragments at higher energies primarily via cleavage of covalent bonds in the cucurbituril. Finally, ion mobility studies show ion populations for the *ortho*- and *meta*-phenylenediamine complexes that primarily have collision cross sections consistent with external complexation, whereas the *para*-phenylenediamine complex has a collision cross section that is smaller, the same as that of protonated cucurbit[6]uril within experimental error. In agreement with experiment, computational studies indicate that at the HF/6-31G* and B3LYP/6-31G*//HF/6-31G* levels of theory external complexation is favored for *ortho*- and *meta*-phenylenediamine, whereas internal complexation is lower in energy for *para*-phenylenediamine. In contrast, MP2/6-31G*//HF-6-31G* calculations predict internal complexation for all three isomers.

1. Introduction

Chemical selectivity, usually involving weak, noncovalent interactions, lies at the heart of all methods of chemical separation and purification. Similar weak interactions are in general responsible for controlling assembly of supramolecular complexes, whether such complexes consist of molecules assembled through biosynthetic pathways or through artificial synthesis. Understanding and benchmarking weak intermolecular interactions is therefore of great current importance.

Gas-phase studies are ideal for probing the fundamental nature of weak intermolecular interactions. The absence of neighboring molecules means that intermolecular interactions of interest can be probed without perturbations that may lead to misconceptions. For example, on the basis of binding constants measured in solution, it was long thought that matching of the size of a crown ether cavity with the size of an alkali metal cation was the basis for selective binding in crown-alkali cation systems.[1] However, because the fundamental interaction in these systems arises between the positive charge of the cation and areas of partial negative charge at the ether oxygen atoms, consideration of the forces involved suggests that the strongest binding should occur for the smallest metal cations, which have the highest charge density and therefore the greatest ability to polarize the ligand. Gas-phase computational[2−5] and experimental[6−12] determinations of the intrinsic binding energies between alkali cations and crown ether hosts show that the fundamental picture is correct; the apparent match between size and binding constants is actually an artifact of the competition between intrinsic binding strengths and solvation energies. Whereas the ion-neutral interactions in this example are relatively strong, much weaker interactions are also amenable to gas-phase study. Further, as this example illustrates nicely, gas-phase experimental data can be directly compared to the results of computational studies. Agreement between the two methods lends confidence to both sets of results. Recent studies calling into question the validity of popular density functional methods for systems involving as few as 10 carbon atoms[13,14] point out the importance of comparing experiment and theory for larger molecular and supramolecular systems.

The host molecule in these studies is cucurbit[6]uril, hereafter abbreviated as CB[6] (Chart 1).[15] CB[6] is a rigid, hollow, barrel-shaped molecule with a height of 9.1 Å, two carbonyl-lined portals with diameters of 3.9 Å, and an interior volume of 164 Å^3.[16] With approximately the right size to accommodate a benzene molecule within its interior cavity, CB[6] is known to have high shape specificity in condensed media,[17] and we expect to see similar shape selectivity in the gas phase, making CB[6] an ideal host for testing ideas about gas-phase characterization of supramolecular systems via mass spectrometry.

With the right size to fit the CB[6] cavity and 1,2-, 1,3-, and 1,4- structural isomers, phenylenediamines (PDAs, Chart 1) are

* To whom correspondence should be addressed. E-mail: david_dearden@byu.edu.
† Brigham Young University.
‡ University of Indiana.
§ University of California, Riverside.

10.1021/jp808771n CCC: $40.75
Published on Web 01/15/2009

CHART 1: Structures and Abbreviations for Cucurbit[6]uril (CB[6]) and the Phenylenediamine (PDA) Isomers

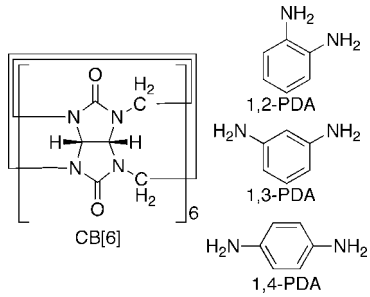

excellent guests to probe the shape specificity of CB[6] in the gas phase. In addition, PDAs are industrially important compounds.[18] All three isomers are used as antiozonants and antioxidants in dye chemistry; in fact, one patent has appeared in the literature dealing with the use of complexes between CB[6] and 1,4-phenylenediamine in cosmetics.[19] The 1,3- and 1,4- isomers are monomers used to synthesize aramid polymers that have high temperature resistance (Nomex, Teijinconex) and very high strength-to-weight ratios (Kevlar, Twaron).[20] When produced by reduction of mixed dinitrobenzenes, the need for separation of the isomers arises.[21] In addition, the PDAs are easily oxidized, so are difficult to maintain in high purity.[18] Efficient means of separating and purifying the PDA isomers could potentially be useful.

Mass spectrometry remains one of the key tools for performing studies on gas-phase species and is increasingly being applied to supramolecular complexes.[22] Usually, observation of a peak at a particular mass-to-charge ratio is used to establish the presence of complexes based on molecular weight, but often it remains difficult to distinguish whether such peaks arise from formation of specific complexes or from nonspecific adduction or other artifacts of transferring species into the gas phase. One of the goals of our research is to develop and apply mass spectrometric methods that will yield additional information about supramolecular systems. For instance, although distinguishing between species with different molecular weights is straightforward, distinguishing between isomers is more challenging. This article addresses the use of molecular recognition techniques to distinguish between isomeric species, with an additional goal of understanding the fundamental basis for isomeric recognition. Tandem mass spectrometric methods have long been used to obtain structural information, particularly about atomic connectivity in molecules; in this article, we use collisional dissociation and chemical reactivity measurements to distinguish supramolecular inclusion complexes from similar complexes in which the guest is bound on the exterior of the host. In addition, we employ ion mobility spectroscopy, which is well-suited to distinguishing between conformers, to confirm the conclusions drawn from the tandem mass spectrometry work.

2. Experimental Section

2.1. Mass Spectrometry. Reactivity and collision-induced dissociation experiments were carried out using a Fourier transform ion cyclotron resonance mass spectrometer[23] (model APEX 47e; Bruker Daltonics, Billerica, MA) equipped with a 4.7 T superconducting magnet. The instrument was controlled by a MIDAS data system[24] (versions 3.18 and 3.20; National High Magnetic Field Laboratory, Tallahassee, FL), and data were processed using the *XMASS* program (version 6.0.2, Bruker Daltonics).

2.2. Materials and Electrospray Conditions. Samples of cucurbit[6]uril (CB[6]), purchased as the dodecahydrate from Fluka (Buchs, Switzerland), were dissolved at concentrations of 1−3 mg mL^{-1} in 88% formic acid. Samples of 1,2-, 1,3-, or 1,4-phenylenediamine (1,2-, 1,3-, or 1,4-PDA; Aldrich, Milwaukee, WI) were dissolved at concentrations of 1−4 mg mL^{-1} in 50:50 methanol/water. Solutions for electrospray were prepared by mixing 100 μL of the CB[6]/formic acid solution and 25−50 μL of the PDA stock solution and then diluting to 1 mL total volume with 50:50 methanol/water. The electrospray source, which has been described,[25] uses a heated capillary inlet, typically maintained at about 50 °C. The typical flow rate for the source was 10 μL hr^{-1}, and the spray needle was typically biased at +1500 V relative to the drying capillary, although these values were adjusted to optimize a stable electrospray signal.

2.3. Collision-Induced Dissociation. Collision-induced dissociation was carried out using the sustained off-resonance irradiation (SORI) method.[26] We isolated the ion of interest using the stored-waveform inverse Fourier transform (SWIFT) technique,[27] tuning the amplitude of the SWIFT pulse to the minimum needed to afford isolation. Isolation was followed by pulsed-valve introduction of Xe collision gas. All experiments were done with a Xe backing pressure of 20 psig and with the valve activated for 6 ms, yielding a peak Xe pressure of about 1×10^{-5} mbar. The gas pulse was immediately followed by single-frequency irradiation 1 kHz below the resonant frequency for the all-^{12}C peak of the ion of interest. The duration of this SORI event was 0.524502 s for each experiment, and the amplitude was varied systematically. Following a 4 s delay to allow the instrument to return to base pressure (10^{-9} mbar), the parent and fragment ions were probed by broadband excitation and detection events.

2.4. Reactivity Studies. The reactivities of the complex ions with *tert*-butylamine were studied by leaking the amine into the vacuum chamber via controlled-variable leak valves (Varian) to a constant pressure of $1-2 \times 10^{-7}$ mbar. The electrosprayed complex ions were isolated using SWIFT and then allowed to react with the neutral amine for a programmatically varied duration. Reactant and product ions were probed via broadband excitation and detection events.

2.5. Computational Methods. Conformational searches were carried out for each complex using the *MacroModel* package (version 7.1; Schrödinger, Inc.; Portland, OR). Searches used the MMFF94S force field supplied with *MacroModel*, with no cutoffs for electrostatic interactions, and employed the MCMM method with 25 000 steps. We used automatic setup for the searches and then disabled torsional rotations within the CB[6] ring. Otherwise, the conformational searches used the *MacroModel* default values.

The lowest-energy structures found in the conformational searches (which were typically found thousands of times) were used as inputs for geometry optimization using ab initio methods. All of these calculations were set up and controlled using the *ECCE* package[28] (version 3.1, Pacific Northwest National Laboratory) and used the computational engine of *NWChem*[29] (version 4.5; Pacific Northwest National Laboratory). Visualization of computed structures was done using the *VMD* package (version 1.8.5).[30] Hartree−Fock (HF) methods were used for full geometry optimization starting from the MMFF structures. We employed the standard 6-31G* basis set in all calculations. This resulted in 1292 basis functions and 2424 primitives for each of the PDA•CB[6] complex ions. Use of

symmetry was enabled with a tolerance of 0.05 Å, and *ECCE/NWChem* defaults were used for all other parameters.

The geometries determined using HF methods were employed to calculate energies via DFT methods, again using the 6-31G* basis set. Symmetry was enabled with 0.05 Å tolerance. We used the B3LYP combined exchange-correlation functionals and *ECCE/NWChem* defaults for all other parameters.

Similarly, energies were calculated at the MP2/6-31G* level using the HF geometries. The frozen core approximation was disabled for these calculations, which otherwise used *ECCE/NWChem* default parameters.

Because of the difficulty in computing vibrational spectra for systems of this size, none of the computed energies are corrected for zero-point energies. For comparison of isomeric systems such as those discussed here, we expect the zero-point corrections to be relatively small.

For calculations of binding energies and comparison of internal versus external complexes, we applied counterpoise corrections[31] for basis set superposition error. The corrections were calculated for the dissociation energies involving removal of doubly protonated phenylenediamine from neutral CB[6]. The difference between dissociation energies for internal versus external complexation then yielded counterpoise-corrected values for the difference in energy between internal and external complexes. The computed corrections were also applied to calculated binding energies for the experimentally observed complex dissociations, which yielded singly protonated CB[6] and singly protonated PDA as products. In general these corrections decreased the binding energies by 20−50 kJ mol^{-1} and were always larger for internal complexes than for external ones. Because of the cost of the calculations, counterpoise corrections were not computed at the MP2 level of theory.

2.6. Ion Mobility Experiments. The experimental cross sections of the cucurbituril-phenylenediamine complexes were determined with an ion mobility instrument that has been described.[32,33] Sample solutions were electrosprayed using 3 kV across a 1 cm gap. The ions were injected into a hexapole for desolvation. The ions were then pulsed into a drift tube for ion mobility measurements. The drift tube potential was 380 V; the collision gas was helium at 4 Torr. The ions exited the drift tube and passed through a quadrupole where they were mass analyzed and detected using microchannel plates. The time required for an ion to travel from the exit of the hexapole to the detector was measured, and the collision cross section Ω was calculated using the following equation.

$$\Omega_{ave}^{(1,1)} = \frac{(18\pi)^{1/2}}{16}\left[\frac{1}{m}+\frac{1}{m_b}\right]^{1/2}\frac{z_e}{(k_B T)^{1/2}}\frac{t_D E}{L}\frac{1}{\rho}$$

Here, m and m_b are the mass of the ion complex and the mass of the collision gas, z_e is the charge of the ion, k_B is the Boltzmann constant, T is temperature in Kelvin, t_D is the drift time, E is the drift field, L is the length of the drift tube, and ρ is the buffer gas number density.

Orientationally averaged, exact hard sphere collision cross sections were also calculated from the lowest-energy structures determined using HF/6-31G* methods. The methods used for these cross section calculations have been described.[34]

3. Results

3.1. Electrospray Mass Spectra. Typical spectra obtained when electrospraying each of the PDA isomers with CB[6] are shown in Figure 1. For 1,2-PDA (part a of Figure 1), the base peak corresponds to a doubly charged 2:1 PDA:CB[6] complex, $[(1,2\text{-PDA}+H)_2\bullet CB[6]]^{2+}$, at *m/z* 607.2. Small peaks are evident at *m/z* 553.2 and 1105.4, corresponding to doubly charged and singly charged 1:1 complexes of 1,2-PDA with CB[6], respectively. Electrospray of 1,3-PDA with CB[6] (part b of Figure 1) again gives a peak at *m/z* 607.2 corresponding to two singly protonated 1,3-PDA molecules attached to CB[6], $[(1,3\text{-PDA}+H)_2\bullet CB[6]]^{2+}$, but the peak at *m/z* 553.2, $[(1,3\text{-PDA}+2H)\bullet CB[6]]^{2+}$, is relatively more intense and the peak at *m/z* 1105.4, the singly protonated complex of 1,3-PDA with CB[6], is the base peak. It is possible to tune the ion source (by using harsher collision conditions) to make the *m/z* 553.2 peak, corresponding to $[(1,3\text{-PDA}+2H)\bullet CB[6]]^{2+}$, dominate the spectrum. Spraying 1,4-PDA with CB[6] (part c of Figure 1) results in a simpler mass spectrum, with almost all of the signal carried by the *m/z* 553.2 peak, corresponding to a doubly protonated complex of 1,4-PDA with CB[6], $[(1,4\text{-PDA}+2H)\bullet CB[6]]^{2+}$. We will show that the last is better represented as an inclusion complex, $[(1,4\text{-PDA}+2H)@CB[6]]^{2+}$, where, following the notation of Smalley, the @ sign denotes inclusion of the molecule preceding the sign into the molecule following the sign.[35]

In summary, complexes of each of the PDA isomers with CB[6] give distinct ESI mass spectra, but it is possible to generate isobaric *m/z* 553.2 ions, corresponding to a doubly charged complex of one PDA molecule with one CB[6], from each of the PDA isomers.

3.2. Reactivity of Doubly Charged Complexes with *tert*-Butylamine. We chose *tert*-butylamine as a reactive probe of the structures of the PDA−CB[6] complexes because previous

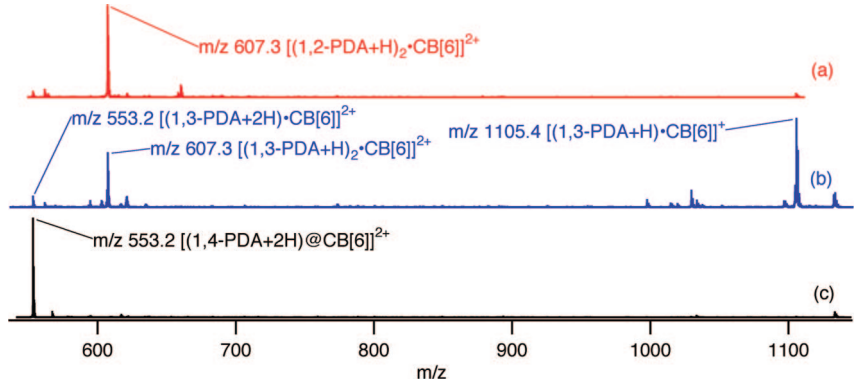

Figure 1. Electrospray ionization Fourier transform ion cyclotron resonance mass spectra of mixtures of cucurbit[6]uril (CB[6]) with 1,2-phenylenediamine (a), 1,3-phenylenediamine (b), and 1,4-phenylenediamine (c).

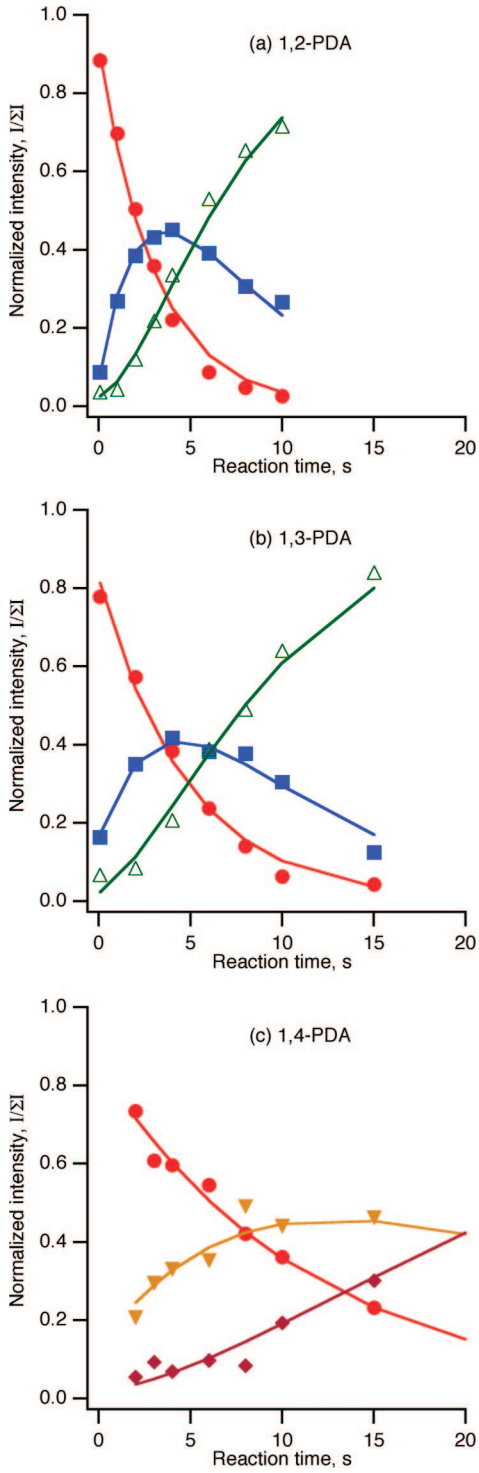

Figure 2. Reactions of *tert*-butylamine with doubly charged PDA−CB[6] complexes. (a) $[(1,2\text{-PDA}+H)_2\bullet CB[6]]^{2+}$ complex; filled circles: $[(1,2\text{-PDA}+H)_2\bullet CB[6]]^{2+}$; filled squares: $[(t\text{-ButNH}_2+H)(1,2\text{-PDA}+H)\bullet CB[6]]^{2+}$; open triangles: $[(t\text{-ButNH}_2+H)_2\bullet CB[6]]^{2+}$. (b) $[(1,3\text{-PDA}+2H)\bullet CB[6]]^{2+}$ complex; filled circles: $[(1,3\text{-PDA}+2H)\bullet CB[6]]^{2+}$; filled squares: $[(t\text{-ButNH}_2+H)(1,3\text{-PDA}+H)\bullet CB[6]]^{2+}$; open triangles: $[(t\text{-ButNH}_2+H)_2\bullet CB[6]]^{2+}$. (c) $[(1,4\text{-PDA}+2H)@CB[6]]^{2+}$ complex; filled circles: $[(1,4\text{-PDA}+2H)@CB[6]]^{2+}$; filled inverted triangles: $(t\text{-ButNH}_2)\bullet[(1,4\text{-PDA}+2H)@CB[6]]^{2+}$; filled diamonds: $(t\text{-ButNH}_2)_2\bullet[(1,4\text{-PDA}+2H)@CB[6]]^{2+}$.

work[36] indicates amines react with ammonium−CB[6] external complexes by replacement, whereas they react with ammonium−CB[6] inclusion complexes by relatively slow addition. Further, the steric bulk of *tert*-butylamine means it is too large to enter the CB[6] cavity. The most abundant doubly charged complexes of each PDA isomer, $[(1,2\text{-PDA}+H)_2\bullet CB[6]]^{2+}$, $[(1,3\text{-PDA}+2H)\bullet CB[6]]^{2+}$, and $[(1,4\text{-PDA}+2H)\bullet CB[6]]^{2+}$, each react with *tert*-butylamine in the gas phase. Each exhibits single-exponential kinetics, suggesting a homogeneous population of ions for each isomer (although a mixture of structures all reacting at similar rates cannot be ruled out). $[(1,2\text{-PDA}+H)_2\bullet CB[6]]^{2+}$ and $[(1,3\text{-PDA}+2H)\bullet CB[6]]^{2+}$ (1:1 and 2:1 PDA−CB[6] complexes, respectively) exhibit similar reactivities, but that of $[(1,4\text{-PDA}+2H)\bullet CB[6]]^{2+}$ (also a 1:1 complex) is distinct from the other two complexes.

TABLE 1: Rate Constants for Reactions with *tert*-Butylamine ($\times 10^{-11}$ cm^3 mol^{-1} s^{-1})

complex	reactions	k_1	k_2
$[(1,2\text{-PDA}+H)_2\bullet CB[6]]^{2+}$	exchange, exchange	11.1 ± 0.5	6.9 ± 0.3
$[(1,3\text{-PDA}+2H)\bullet CB[6]]^{2+}$	addition, exchange	6.3 ± 0.4	5.6 ± 0.5
$[(1,4\text{-PDA}+2H)@CB[6]]^{2+}$	addition, addition	5.2 ± 0.4	1.2 ± 0.2

A kinetic plot showing the reaction of *tert*-butylamine with $[(1,2\text{-PDA}+H)_2\bullet CB[6]]^{2+}$ is given in part a of Figure 2, and rate constants extracted from the kinetic data are compiled in Table 1. The amine rapidly displaces first one and then the second 1,2-PDA molecule from the complex. The first exchange is about twice as fast as the second, as expected for two independent exchange processes where the first is statistically twice as likely as the second.

The reactions between $[(1,3\text{-PDA}+2H)\bullet CB[6]]^{2+}$ and *tert*-butylamine are shown in part b of Figure 2. For this complex, *tert*-butylamine first adds to the complex, followed by exchange of a second *tert*-butylamine for 1,3-PDA, such that the final product has the same *m*/*z* as was observed in the reactions of the 1,2-PDA complex. We assume this product is $[(t\text{-ButNH}_2+H)_2\bullet CB[6]]^{2+}$. The rate of the exchange is similar to that of the second exchange for the 1,2-PDA complex described above.

The $[(1,4\text{-PDA}+2H)@CB[6]]^{2+}$ complex exhibits reactivity with *tert*-butylamine (part c of Figure 2) that is distinct from that of the other two complexes. Rather than exchanging amines as do the other two complexes, this complex undergoes sequential addition of two molecules of *tert*-butylamine. The first addition is relatively rapid, with a rate comparable to the addition rate observed for the 1,3-PDA complex, whereas the second addition is about a factor of 4 slower.

3.3. Sustained Off-Resonance Irradiation Collision-Induced Dissociation (SORI-CID). Our previous work with CB[6]-diammonium complexes[36] suggests that the SORI-CID spectra of complexes that do not involve inclusion are significantly simpler than those that do. We therefore performed SORI-CID experiments on doubly charged PDA-CB[6] complexes, with the results summarized in Figure 3. Ideally, it would have been desirable to compare the doubly charged, 1:1 PDA-CB[6] complexes for the three isomers, but ESI did not produce such 1,2- or 1,3-PDA complexes with sufficient abundance for SORI-CID (Figure 1); hence, we examine doubly charged 2:1 complexes of 1,2- and 1,3-PDA, as well as the doubly charged 1:1 complex of 1,4-PDA with CB[6].

Excitation of the $[(1,2\text{-PDA}+H)_2\bullet CB[6]]^{2+}$ complex (*m*/*z* 607.2) 1 kHz off resonance results in the SORI-CID spectrum shown in part a of Figure 3. Only two dissociation products are evident in this simple spectrum, corresponding to $[CB[6]+H]^+$ at *m*/*z* 997.4 and $[(1,2\text{-PDA}+H)\bullet CB[6]]^+$ at *m*/*z* 1105.5. These ionic products formally involve losses from the complex of the protonated dimer and monomer of 1,2-PDA, respectively. Production of $[CB[6]+H]^+$ could also arise from

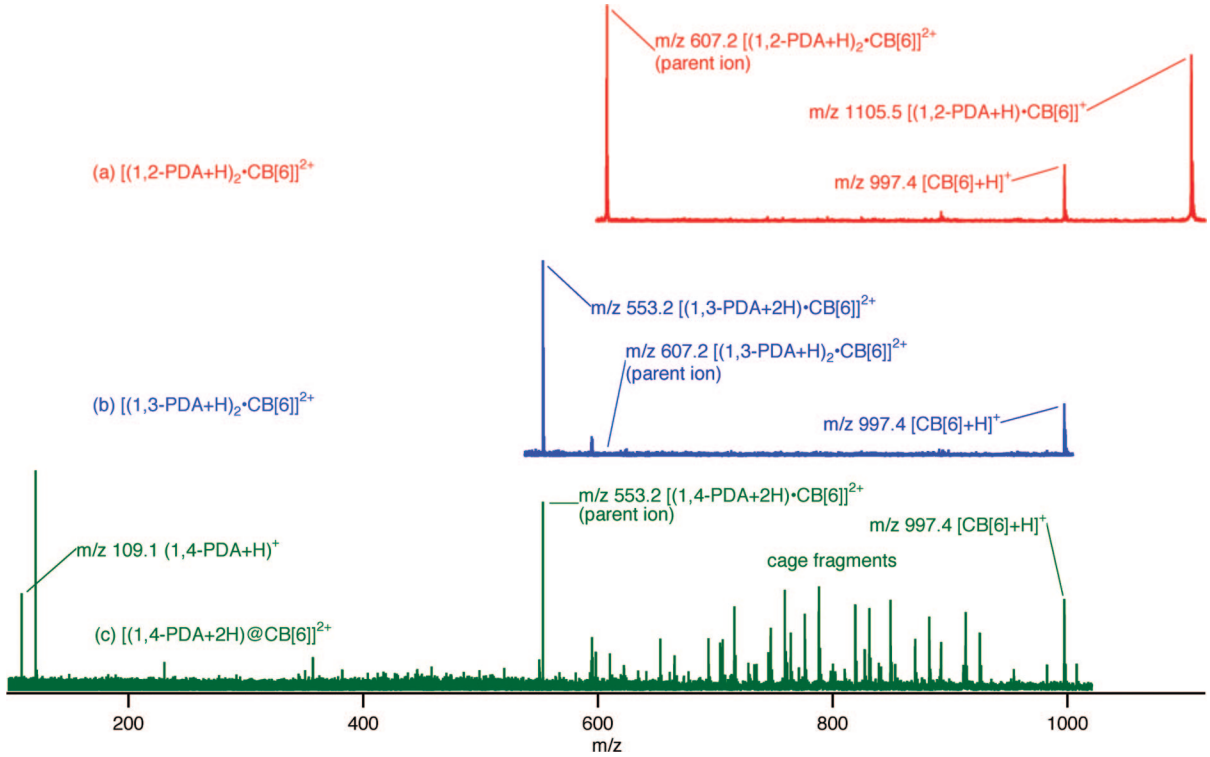

Figure 3. Sustained off-resonance irradiation collision-induced dissociation spectra of (a) $[(1,2\text{-PDA}+H)_2\bullet CB[6]]^{2+}$, (b) $[(1,3\text{-PDA}+H)_2\bullet CB[6]]^{2+}$, and (c) $[(1,4\text{-PDA}+2H)@CB[6]]^{2+}$.

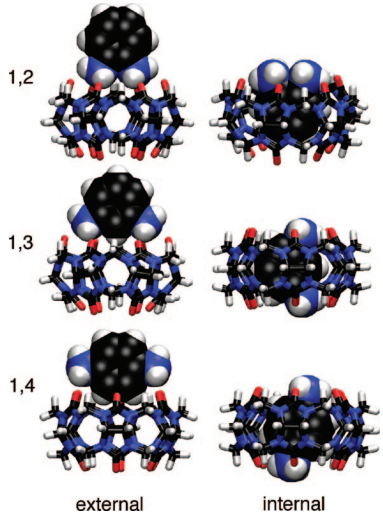

Figure 4. Structures of lowest-energy computed HF/6-31G* external and internal 1:1, doubly charged complexes of phenylenediamine isomers (space filling) with cucurbit[6]uril (tubes).

sequential losses of neutral and protonated 1,2-PDA (in either order); our experiments do not identify which pathway is actually followed. The complementary singly charged product ion, $[1,2\text{-PDA}+H]^+$, was not observed. This kind of discrimination against low *m/z* product ions is common in FTICR SORI-CID spectra.

Excitation of the $[(1,3\text{-PDA}+H)_2\bullet CB[6]]^{2+}$ complex (*m/z* 607.2) 1 kHz off resonance yields a similar set of fragment ions. At low excitation amplitudes, the only product ion is one at *m/z* 553.2, corresponding to loss of one neutral 1,3-PDA molecule from the complex, resulting in an ion with the $[(1,3\text{-PDA}+2H)\bullet CB[6]]^{2+}$ stoichiometry. At higher excitation amplitudes (part b of Figure 3), a second product ion appears, corresponding to protonated CB[6] at *m/z* 997.4. Again, the low *m/z* complementary singly charged ion was not observed.

The $[(1,4\text{-PDA}+2H)\bullet CB[6]]^{2+}$ ion (*m/z* 553.2), excited 1 kHz off resonance, yields a much more complex set of product ions. These include protonated 1,4-PDA at *m/z* 109.1, protonated CB[6] at *m/z* 997.4, and a number of ions corresponding to fragmentation of the CB[6] cage. These results are similar to those seen previously for the complex of 1,4-butanediammonium with CB[6], which is believed to involve inclusion of the diammonium ion within the CB[6] cavity.[36] Although these experiments do not yield quantitative threshold information, we also note that SORI amplitudes roughly twice as high are required to produce dissociation of the $[(1,4\text{-PDA}+2H)\bullet CB[6]]^{2+}$ ion as were required for the $[(1,3\text{-PDA}+H)_2\bullet CB[6]]^{2+}$ complex.

3.4. Computational Results. The structures of the lowest-energy internal and external 1:1 doubly charged complexes of the phenylenediamine isomers found at the HF/6-31G* level of theory are shown in Figure 4. The corresponding relative energies at various levels of theory are compiled in Table 2. Differences between the energies of the internal and external complexes are reported both as calculated directly from the Hartree−Fock or DFT energy differences and with counterpoise corrections included. Because the counterpoise corrections are always larger for the internal complexes than for the external complexes (as expected given that basis set superposition is greater for internal complexes than for external complexes), the effect of including the counterpoise corrections is to make the difference between internal and external energies more positive.

At each level of theory, the internal $[(1,4\text{-PDA}+2H)@CB[6]]^{2+}$ complex is lowest in energy. Each level of theory gives the same energetic ordering for the internal complexes, 1,2-PDA > 1,3-PDA > 1,4-PDA, and for the external complexes, 1,4-PDA > 1,2-PDA > 1,3-PDA. All three levels of theory are in reasonable agreement for the relative energies of the internal and external complexes taken separately, and HF/6-31G* and B3LYP/6-31G*//HF/6-31G* are in good

TABLE 2: Computed Relative Energies of Doubly-Charged 1:1 Complexes of Phenylenediamine (PDA) Isomers with cucurbit[6]uril (kJ mol^{-1})

	HF/6-31G*		B3LYP/6-31G*//HF/6-31G*						MP2/6-31G*// HF/6-31G*	
guest	internal	external	Δ_{direct}[a]	Δ_{CP}[b]	internal	external	Δ_{direct}[a]	Δ_{CP}[b]	internal	external
1,2-PDA	137	40	97	121	115	38	77	103	128	169
1,3-PDA	62	25	37	55	46	29	17	37	48	143
1,4-PDA	0	87	−87	−69	0	85	−85	−67	0	208

[a] Energy of internal complex − energy of external complex [b] Counterpoise corrected difference, from the difference in binding energies of internally and externally bound guest, $D(\text{CB[6]}{-}\text{PDA}{+}2\text{H}^{2+})_{internal} - D(\text{CB[6]}{-}\text{PDA}{+}2\text{H}^{2+})_{external}$, using counterpoise corrected values for the dissociation energies.

TABLE 3: HF/6-31G* Computed O−O Cross-Portal Distances (Å) for Internally-Bound PDA Isomers

guest	maximum	minimum	difference
none (free CB[6])	7.152	7.152	0
1,2-PDA	7.946	5.637	2.309
1,3-PDA	7.226	5.774	1.452
1,4-PDA	6.984	5.975	1.009

agreement for relative energies for all the complexes, but the MP2/6-31G*//HF/6-31G* relative values for the external complexes are significantly (about 120 kJ mol^{-1}) higher than those from the other two methods. The reasons for this disagreement are not clear. These high values mean that, at the MP2 level of theory, internal binding is preferred for all three PDA isomers, although the preference for internal binding increases in the order 1,2-PDA < 1,3-PDA < 1,4-PDA, in accord with the other levels of theory. What is clear from all three levels of theory is that the preference of CB[6] for external binding of 1,2-PDA is greatest, and for internal binding of 1,4-PDA is greatest, with internal and external binding being most similar for the 1,3-PDA isomer.

Visual inspection of Figure 4 suggests differing degrees of CB[6] portal distortion in the inclusion complexes, and this is borne out by measurements of the opposing O−O distances across the portals of the various complexes (Table 3). Insertion of any of the phenylenediamine isomers into CB[6] results in stretching of CB[6] in the direction of the plane defined by the phenylenediamine π ring and puckering in the orthogonal direction. This effect is greatest for 1,2-PDA and least for 1,4-PDA; the latter is most like the free CB[6] host.

3.5. Ion Mobility. Computed (exact hard sphere) and measured collision cross sections for various observed PDA−CB[6] complexes are given in Table 4. Computed cross sections for the external complexes are about 10% larger than for the internal complexes, suggesting that cross section measurements should easily be able to distinguish between internal and external binding.

Ion populations probed using the ion mobility instrument were almost certainly not identical to those studied using the ESI-FTICR. In particular, the ion mobility instrument used larger electrospray potentials and harsher desolvation conditions than the ESI-FTICR. It is therefore likely that the ions in the mobility experiments experienced a higher energy environment than those in the ESI-FTICR; as a result, the mass spectra obtained on the ion mobility instrument tended to consist of low mass fragments and higher mass species in the *m*/*z* range expected for singly charged complexes (mass resolution was not sufficient to directly determine charge states), in contrast to the ESI-FTICR spectra in Figure 1, which include abundant doubly and singly charged complex ions.

Singly charged 1:1 PDA-CB[6] complexes were observed for all three PDA isomers as well as for singly protonated CB[6] (Figure 5). Protonated CB[6] has an arrival time peaking at about 3000 μs, corresponding to a measured collision cross section of 178 Å^2. Two peaks appeared in the arrival time distributions for each complex. In each of these cases, one of the peaks has the same arrival time and collision cross section as protonated CB[6], consistent with an internal complex. Each of the singly charged 1:1 PDA−CB[6] complexes also exhibits a peak with an arrival time distribution peaking around 3400 μs, corresponding to a collision cross section of about 200 Å^2, consistent with binding of the PDA on the exterior of CB[6].

A doubly charged 1:1 complex was observed only in the case of the 1,4-PDA guest. This ion yielded a bimodal arrival time distribution, with the first peak having the same collision cross section as protonated CB[6], consistent with an internal complex. The second peak corresponds to a 256 Å^2 cross section, much larger than expected for any 1:1 PDA−CB[6] complex. This ion could arise from a doubly charged 2:1 PDA−CB[6] complex that dissociates after the mobility cell but prior to mass analysis. Its arrival time distribution is similar to that observed for the *m*/*z* 607 ion, which is assigned as $[(1,4\text{-PDA}{+}\text{H})_2{\bullet}\text{CB[6]}]^{2+}$, and the corresponding *m*/*z* 607 ion arising from 1,3-PDA does dissociate to yield an ion at *m*/*z* 553 consistent with a doubly charged, 1:1 complex (Figure 3). More work will be required to sort out the proper assignment for this peak. Both the 1,2- and 1,3-PDA guests also yielded doubly charged 2:1 PDA−CB[6] complexes that have cross sections about 10% larger than were observed for the 1:1 complexes. These are consistent with both of the PDA species binding on the exterior of CB[6].

4. Discussion

4.1. Distinguishing External and Internal Complexes by Mass Spectrometry. The experimental and computational results presented above are consistent with external binding of doubly protonated 1,2- and 1,3-PDA by CB[6], and internal binding of doubly protonated 1,4-PDA. The former two complexes constitute minor ions in the ESI mass spectra of PDA-CB[6] mixtures, whereas the doubly charged *m*/*z* 553.2 ion, corresponding to internal $[(1,4\text{-PDA}{+}2\text{H})@\text{CB[6]}]^{2+}$, dominates the spectrum when 1,4-PDA and CB[6] are electrosprayed together. This is consistent with a stable internal complex for 1,4-PDA and collisionally labile external complexes for the other two PDA isomers.

The reactivity results are also consistent with this interpretation. In particular, the *m*/*z* 553.2 ions arising from complexes of 1,3- and 1,4-PDA with CB[6] exhibit distinct reactivity with *tert*-butylamine. The 1,3-PDA complex adds one molecule of *tert*-butylamine and then the 1,3-PDA is rapidly displaced by a second molecule of *tert*-butylamine. In contrast, the 1,4-PDA complex never loses the phenylenediamine, but instead adds two molecules of *tert*-butylamine, much as was previously observed for the internal complex of 1,4-butanediammonium with CB[6].[36] The caged guest is difficult to displace, whereas externally bound amines are easily exchanged.

TABLE 4: Computed and Measured Collision Cross Sections for Phenylendiamine−cucurbit[6]uril Complexes (Å^2)

Guest	Computed		Experimental		
	1:1, internal	1:1, external	1:1, +1 (*m*/*z* 1105)	1:1, +2 (*m*/*z* 553)	2:1, +2 (*m*/*z* 607)
H^+			178[a]		
1,2-PDA	187	207	178(46%), 199(54%)	not observed	218
1,3-PDA	185	203	198	not observed	220
1,4-PDA	184	201	177(68%), 200(32%)	178(60%), 256(40%)	269

[a] Observed at *m*/*z* 997.

TABLE 5: Computed Dissociation Energies *D*(CB[6]H$^+$−PDAH$^+$) (kJ mol^{-1})

		HF/6-31G*		B3LYP/6-31G*//HF/6-31G*	
guest	binding site	uncorrected	with CP correction	uncorrected	with CP correction
1,2-PDA	internal	42	5	67	17
1,2-PDA	external	139	126	143	120
1,3-PDA	internal	136	99	147	97
1,3-PDA	external	172	154	164	135
1,4-PDA	internal	191	156	186	138
1,4-PDA	external	104	87	101	71

TABLE 6: Contributions to Dissociation Energy for Complexes of Cucurbit[6]uril (CB[6]) with Phenylenediamine (PDA) Isomers (kJ mol^{-1})[a]

complex	binding site	*D*[CB[6]−(PDA+2H)$^{2+}$]	CB[6] relaxation	PDA relaxation	total relaxation	interaction
1,2-PDA	internal	596	−53	−28	−81	677
1,2-PDA	external	699	−50	−9	−60	759
1,3-PDA	internal	581	−77	−17	−94	675
1,3-PDA	external	619	−47	−8	−54	673
1,4-PDA	internal	613	−75	−7	−82	695
1,4-PDA	external	545	−30	−9	−40	585

[a] Computed at the B3LYP/6-31G*//HF/6-31G* level of theory, with counterpoise corrections included.

The collisional dissociation data are also consistent with external complexation by 1,2- and 1,3-PDA; these complexes are easily dissociated via loss of the neutral or protonated amine. In the case of the 1,3-PDA complexes, the SORI-CID results suggest that any observed doubly charged, 1:1 complex may be the result of collisional dissociation in the ion source, as dissociation of $[(1,3\text{-PDA}+H)_2\bullet CB[6]]^{2+}$ yields $[(1,3\text{-PDA}+2H)\bullet CB[6]]^{2+}$, which is in turn easily dissociated to give protonated CB[6]. In contrast, higher collisional energies are required to induce dissociation of the 1,4-PDA complex, such that loss of the amine is competitive with fragmentation of the covalent framework of the CB[6] cage. Again, this is in close analogy with the previously observed behavior of the internal 1,4-butanediammonium complex of CB[6].[36]

The ion mobility results provide the most straightforward experimental evidence for internal versus external binding. Unfortunately, signal levels for the doubly charged 1:1 complexes were not sufficient to characterize the doubly charged complexes involving 1,2- or 1,3-PDA. However, the singly charged species still give some indication of whether internally bound or externally bound complexes are favored. The 200 Å^2 cross section ions, in good agreement with computed cross sections for external complexes, represent the majority of the ion population for the singly charged 1:1 PDA:CB[6] complexes involving 1,2- and 1,3-PDA (Table 4). On the other hand, 68% of the singly charged 1:1 1,4-PDA:CB[6] complex has the same cross section as protonated CB[6] (around 180 Å^2) and is most likely an internally bound complex. The observed doubly charged 1:1 complex, the $[(1,4\text{-PDA}+2H)@CB[6]]^{2+}$ ion, has the same cross section as protonated CB[6], consistent with an internal complex. As in Tolkein's novels, wearing the CB[6] ring makes the appropriately shaped 1,4-PDA wearer invisible, at least as far as collision cross sections are concerned!

The experimental results are in agreement with the results of HF/6-31G* and B3LYP/6-31G*//HF/6-31G* computational studies (Table 2). At the DFT level of theory with counterpoise corrections included, the external 1,2-PDA complex is 103 kJ mol^{-1} lower in energy than the internal complex, and similarly the external 1,3-PDA complex is 37 kJ mol^{-1} lower in energy than the corresponding internal complex. On the other hand, at the same level of theory the *internal* 1,4-PDA complex is 67 kJ mol^{-1} lower in energy than the external complex, probably reflecting the greatest spatial separation between the charges, combined with solvation of the charges by the CB[6] ligand, which is optimal in this complex.

Finally, we cannot rule out the possibility that the observed ion populations consist of mixtures of internally and externally bound complexes. The ESI-FTICR experiments are relatively insensitive to the presence of mixtures. The ion mobility data (Table 4) provide the best available experimental probe of the size distributions within the various ion populations. For the singly charged 1:1 complexes, those experiments suggest the 1,2-PDA complexes are indeed a mixture of internally- and externally bound species, with roughly equal populations. For 1,3-PDA, only the externally bound 1:1 complex was observed, whereas for 1,4-PDA both externally and internally bound complexes were detected, with the internally bound species twice as abundant as the externally bound ones. The only doubly charged 1:1 complex for which data were obtained, involving 1,4-PDA, consists at least 60% of internally bound species and may actually be 100% internally bound if the 256 Å^2 complex is due to dissociating $[(1,4\text{-PDA}+H)_2\bullet CB[6]]^{2+}$, as suggested above.

4.2. Dissociation Energies. The experimentally observed dissociation behavior is consistent with the computational results (Table 5). Dissociation of the external complexes involving 1,2-

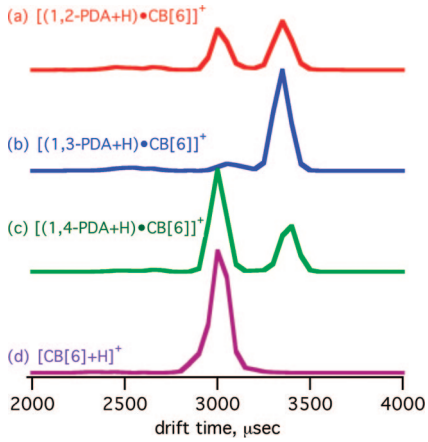

Figure 5. Arrival time distributions for singly charged complexes of cucurbit[6]uril with (a) 1,2-phenylenediamine; (b) 1,3-phenylenediamine; (c) 1,4-phenylenediamine; and (d) H^+.

and 1,3-PDA, which have the lowest computed dissociation energies, is facile, whereas dissociation of the internal $[(1,4\text{-PDA}+2H)@CB[6]]^{2+}$ complex, with a higher computed dissociation energy, is not. For every PDA isomer, the computed dissociation energy for production of $CB[6]H^+$ and $PDAH^+$ products is far lower than that required for leaving both charges on the phenylenediamine, in accordance with observation.

Even the highest computed dissociation energy for the internal $[(1,4\text{-PDA}+2H)@CB[6]]^{2+}$ complex dissociating to singly protonated components (191 kJ mol^{-1}, at the uncorrected HF/6-31G* level of theory) is small enough that it might be surprising this is not the dominant process upon collisional activation. In fact, dissociation of $[(1,3\text{-PDA}+2H)•CB[6]]^{2+}$ (part b of Figure 3), with a very similar computed energy cost (Table 5), does occur via simple loss of protonated 1,3-PDA. All other fragmentation routes would involve breaking covalent bonds, which would certainly involve higher energies than those shown in Table 5. However, the fact that 1,4-PDA is included within the cucurbituril must create a significant barrier to dissociation, such that decomplexation and covalent fragmentation of the cage are competitive processes when the guest is caged. Decomplexation would require the rupture of all of the hydrogen bonds holding the complex together, along with motion of the guest in the proper direction to exit the host. Likely, the entropic cost of this process disfavors it relative to covalent cleavage of the CB[6] cage.

4.3. Factors Accounting for Shape Recognition in Complexes of Cucurbit[6]uril with Phenylenediamine Isomers. Solution data provide good precedent for the large size and shape selectivity of the CB[6] host. In 1:1 water−formic acid solution, CB[6] binds 4-methylbenzylamine with a binding constant K_a of 320 M^{-1}, whereas no binding was detected for the 2- and 3-methyl isomers,[15] probably because they cannot easily fit within the CB[6] cavity. The present work shows that similar shape selectivity exists for gas-phase complexes. Assuming these systems are under thermodynamic control, what accounts for this selectivity? Some insight comes from a closer look at the computational results.

Counterpoise corrections involve calculation of the energies of reactant and product species all using identical basis sets at the geometry of the complex, with separate calculation of the energy required to convert the reactants from their fully relaxed geometries to the geometries they adopt in the complex. Thus, analysis of the results of these calculations allows estimation of the strain induced by complexation and of the energy gained

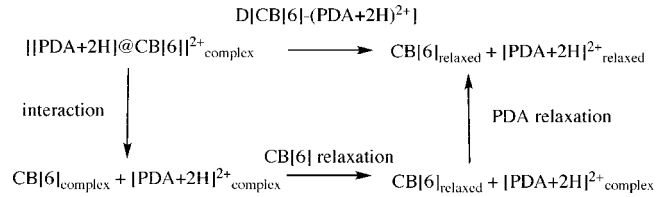

Figure 6. Thermodynamic cycle linking relaxation energy and interaction energy with dissociation energy for the reaction of doubly protonated phenylenediamine (PDA) with neutral cucurbit[6]uril (CB[6]).

by allowing the host and guest to interact, forming a thermodynamic cycle with the binding energy (Figure 6). In these calculations, both protons remain closely associated with the phenylenediamine throughout the process. This is not the experimentally observed lowest energy pathway, but because energy is a thermodynamic state function it is still conceptually useful for understanding the overall energetics of complexation.

Table 6 shows the computed energies associated with each of the steps depicted in Figure 6 for internal and external complexes of each of the phenylenediamine isomers with cucurbit[6]uril. The relaxation energies are the energies released on relaxing each component from the conformation adopted in the complex to the lowest-energy conformation of the free host or guest. Thus, they reflect the energetic cost of adopting the proper conformation for binding. The interaction energies are the energy differences between the complex and the separated host and guest, each remaining in the conformation it adopts in the complex. From the data in the table, it is clear that the energy of interaction between host and guest is by far the largest contribution to the overall dissociation energy. The magnitude of the relaxation energies is greater for internal complexation than for external complexation, reflecting the more restrictive geometric and steric requirements for both host and guest to allow binding in the internal binding site. The magnitude of the CB[6] relaxation energy is 2−10 times larger than that for any of the PDA guests, in accordance with the greater ability of the larger host to adapt to the smaller guest than vice versa. For 1,2- and 1,4-PDA, the binding site preference arises primarily from the interaction energy, favoring external and internal binding for 1,2- and 1,4-PDA, respectively. For the 1,3-isomer, the interaction energies in the two binding sites are similar, and the small preference for external binding occurs because less strain is associated with the external site than with the internal one. Overall, complementarity between the binding domains on the host and guest leading to favorable binding enthalpy is the most important factor in the shape selectivity of CB[6] for the PDA isomers, with strain in the host and guest playing a secondary role.

Finally, it is interesting to compare binding preferences in solution to the gas-phase trends examined here. As noted above, the trends for isomeric methylbenzylamine complexes of CB[6] in solution are qualitatively similar to the gas-phase trends reported here for the isomeric phenylenediamines. However, the driving forces behind the trends can be quite different in the two environments. In solution, at least some of the driving force for host−guest binding often arises because expulsion of solvent from the host binding cavity, and/or disruption of interactions between solvent and guest, is entropically favorable. If the guest has difficulty entering the host cavity, as in the example of the methylbenzylamine complexes noted above, no solvent is expelled, entropic benefits are decreased, and complexation may not be observed. In the gas phase, no entropic stabilization from liberation of solvent is available. Rather, the

loss of translational freedom that occurs upon complexation is always unfavorable. Restriction of vibrational and/or rotational degrees of freedom on complex formation is also unfavorable. Hence, entropy frequently favors complex formation in solution, but always disfavors complexation in the absence of solvent.

Enthalpy can either favor or disfavor complexation in solution, depending on the balance between solvation enthalpies of host and guest and the interaction enthalpy associated with complex formation. On the other hand, in the gas phase there is no competition between solvation and complex formation, so interaction enthalpy is always favorable and tends to be the dominant factor in gas-phase complexation. As a result, it is much easier to form nonspecific complexes in the gas phase than in solution, and in fact such nonspecific complexes are often observed in electrospray mass spectrometry.

5. Conclusions

Simple observation of a peak at a particular *m*/*z* value in a mass spectrum reveals little about the nature of a complex ion other than its existence. However, the use of tandem methods, specifically reactivity measurements and observation of the collision-induced fragmentation pattern, can distinguish between internal and external binding sites, as confirmed by ion mobility techniques that measure collision cross sections. Given the inherent sensitivity and speed of mass spectrometry, the use of such tandem methods should be attractive to those interested in characterizing supramolecular complexes beyond confirming their presence.

For the systems studied here, experiments are in good agreement with HF and B3LYP computational approaches with a moderate-sized basis set. It is encouraging to find that these methods yield useful results for larger-than-usual systems. However, it remains unclear why MP2 methods fail to predict the observed preference of 1,2- and 1,3-phenylenediamine to bind on the exterior of CB[6]. More work is needed to determine whether these results are anomalous or if there is a deeper problem with applying perturbation theory to larger systems.

Acknowledgment. We are grateful for support of this work by the U.S. National Science Foundation (CHE-0615964) and for computer time from the Ira and Marylou Fulton Supercomputing Center at Brigham Young University.

Supporting Information Available: Energies and Cartesian coordinates for computed stationary points. This material is available free of charge via the Internet at http://pubs.acs.org.

References and Notes

(1) Izatt, R. M.; Pawlak, K.; Bradshaw, J. S.; Bruening, R. L. *Chem. Rev.* **1991**, *91*, 1721–2085.
(2) Glendening, E. D.; Feller, D.; Thompson, M. A. *J. Am. Chem. Soc.* **1994**, *116*, 10657–10669.
(3) Hill, S. E.; Feller, D.; Glendening, E. D. *J. Phys. Chem. A* **1998**, *102*, 3813–3819.
(4) Hill, S. E.; Glendening, E. D.; Feller, D. *J. Phys. Chem. A* **1997**, *101*, 6125–6131.
(5) Hill, S. E.; Feller, D. *Int. J. Mass Spectrom.* **2000**, *201*, 41–58.
(6) More, M. B.; Glendening, E. D.; Ray, D.; Feller, D.; Armentrout, P. B. *J. Phys. Chem.* **1996**, *100*, 1605–1614.
(7) Ray, D.; Feller, D.; More, M. B.; Glendening, E. D.; Armentrout, P. B. *J. Phys. Chem.* **1996**, *100*, 16116–16125.
(8) More, M. B.; Ray, D.; Armentrout, P. B. *J. Phys. Chem. A* **1997**, *101*, 831–839.
(9) More, M. B.; Ray, D.; Armentrout, P. B. *J. Phys. Chem. A* **1997**, *101*, 7007–7017.
(10) More, M. B.; Ray, D.; Armentrout, P. B. *J. Phys. Chem. A* **1997**, *101*, 4254–4262.
(11) Armentrout, P. B. *Int. J. Mass Spectrom.* **1999**, *193*, 227–240.
(12) More, M. B.; Ray, D.; Armentrout, P. B. *J. Am. Chem. Soc.* **1999**, *121*, 417–423.
(13) Grimme, S. *Angew. Chem., Int. Ed.* **2006**, *45*, 4460–4464.
(14) Schreiner, P. R.; Fokin, A. A.; Pascal, R. A., Jr.; de Meijere, A. *Org. Lett.* **2006**, *8*, 3635–3638.
(15) Lagona, J.; Mukhopadhyay, P.; Chakrabarti, S.; Isaacs, L. *Angew. Chem., Int. Ed.* **2005**, *44*, 4844–4870.
(16) Lee, J. W.; Samal, S.; Selvapalam, N.; Kim, H.-J.; Kim, K. *Acc. Chem. Res.* **2003**, *36*, 621–630.
(17) Mock, W. L. In *Comprehensive Supramolecular Chemistry*; Vögtle, F., Ed.; Elsevier: New York, 1996; Vol. 2, pp 477−493.
(18) Smiley, R. A. In *Ullmann's Encyclopedia of Industrial Chemistry*; Elvers, B., Hawkins, S., Schulz, G., Eds.; VCH: Weinheim, Germany, 1991; Vol. A19, p 405−410.
(19) Hoeffkes, H.; Knuebel, G.; Giesa, H. *Cosmetic Agents Containing Macrocycles Selected from the Group of Cucurbituril and Hemicucurbituril Derivatives*. Germany Appl. DE 2006−102006011317, 3 Sept. 2006.
(20) Tanner, D.; Fitzgerald, J. A.; Phillips, B. R. *Angew. Chem., Int. Ed.* **1989**, *28*, 649–654.
(21) Kamble, S. P.; Gaikar, V. G. *Sep. Sci. Technol.* **2003**, *38*, 3409–3430.
(22) Schalley, C. A. *Int. J. Mass Spectrom.* **2000**, *194*, 11–39.
(23) Dearden, D. V.; Dejsupa, C.; Liang, Y.; Bradshaw, J. S.; Izatt, R. M. *J. Am. Chem. Soc.* **1997**, *119*, 353–359.
(24) Senko, M. W.; Canterbury, J. D.; Guan, S.; Marshall, A. G. *Rapid Commun. Mass Spectrom.* **1996**, *10*, 1839–1844.
(25) Wigger, M.; Nawrocki, J. P.; Watson, C. H.; Eyler, J. R.; Benner, S. A. *Rapid Commun. Mass Spectrom.* **1997**, *11*, 1749–1752.
(26) Bakhtiar, R.; Holznagel, C. M.; Jacobson, D. B. *Organometallics* **1993**, *12*, 621–623.
(27) Chen, L.; Wang, T.-C. L.; Ricca, T. L.; Marshall, A. G. *Anal. Chem.* **1987**, *59*, 449–454.
(28) Black, G.; Didier, B.; Feller, D.; Gracio, D.; Hackler, M.; Havre, S.; Jones, D.; Jurrus, E.; Keller, T.; Lansing, C.; Matsumoto, S.; Palmer, B.; Peterson, M.; Schuchardt, K.; Stephan, E.; Taylor, H.; Thomas, G.; Vorpagel, E.; Windus, T.; Winters, C. *Ecce, A Problem Solving Environment for Computational Chemistry*; Pacific Northwest National Laboratory: Richland, WA, 2003.
(29) Straatsma, T. P.; Apra, E.; Windus, T. L.; Dupuis, M.; Bylaska, E. J.; de Jong, W.; Hirata, S.; Smith, D. M. A.; Hackler, M. T.; Pollack, L.; Harrison, R. J.; Nieplocha, J.; Tipparaju, V.; Krishnan, M.; Brown, E.; Cisneros, G.; Fann, G. I.; Fruchtl, H.; Garza, J.; Hirao, K.; Kendall, R.; Nichols, J. A.; Tsemekhman, K.; Valiev, M.; Wolinski, K.; Anchell, J.; Bernholdt, D.; Borowski, P.; Clark, T.; Clerc, D.; Dachsel, H.; Deegan, M.; Dyall, K.; Elwood, D.; Glendening, E.; Gutowski, M.; Hess, A.; Jaffe, J.; Johnson, B.; Ju, J.; Kobayashi, R.; Kutteh, R.; Lin, Z.; Littlefield, R.; Long, X.; Meng, B.; Nakajima, T.; Niu, S.; Rosing, M.; Sandrone, G.; Stave, M.; Taylor, H.; Thomas, G.; van Lenthe, J.; Wong, A.; Zhang, Z. *NWChem, A Computational Chemistry Package for Parallel Computers*; Pacific Northwest National Laboratory: Richland, 2003.
(30) Humphrey, W.; Dalke, A.; Schulten, K. *J. Mol. Graphics* **1996**, *14*, 33–38.
(31) Boys, S. F.; Bernardi, F. *Mol. Phys.* **1970**, *19*, 553–566.
(32) Kohtani, M.; Jones, T. C.; Schneider, J. E.; Jarrold, M. F. *J. Am. Chem. Soc.* **2004**, *126*, 7420–7421.
(33) Kinnear, B. S.; Hartings, M. R.; Jarrold, M. F. *J. Am. Chem. Soc.* **2001**, *123*, 5660–5667.
(34) Shvartsburg, A. A.; Jarrold, M. F. *Chem. Phys. Lett.* **1996**, *261*, 86–91.
(35) Chai, Y.; Guo, T.; Jin, C. M.; Haufler, R. E.; Chibante, L. P. F.; Fure, J.; Wang, L. H.; Alford, J. M.; Smalley, R. E. *J. Phys. Chem.* **1991**, *95*, 7564–7568.
(36) Zhang, H.; Paulsen, E. S.; Walker, K. A.; Krakowiak, K. E.; Dearden, D. V. *J. Am. Chem. Soc.* **2003**, *125*, 9284–9285.

JP808771N